# The blue halite in Morsleben, Germany: A natural lyoluminescence dosimeter?

Magdalena Biernacka, Renata Majgier, Krzysztof Staninski, Malgorzata Kaczmarek, Sylwia Zelek-Pogudz, Michal Sądel, Katarzyna M Szufa, Hartmut Blanke, Sebastian Kreutzer

Journal of Luminescence 280 (2025) 121088

Contents lists available at ScienceDirect

Journal of Luminescence

journal homepage: www.elsevier.com/locate/jlumin

Full Length Article

# The blue halite in Morsleben, Germany: A natural lyoluminescence dosimeter?

Magdalena Biernacka [a,b,*], Renata Majgier [c], Krzysztof Staninski [d], Małgorzata Kaczmarek [d], Sylwia Zelek-Pogudz [e], Michał Sądel [f], Katarzyna M. Szufa [c], Hartmut Blanke [g], Sebastian Kreutzer [a]

[a] Institute of Geography, Heidelberg University, Im Neuenheimer Feld 348, 69120, Heidelberg, Germany
[b] Institute of Physics, Faculty of Physics, Astronomy and Informatics, Nicolaus Copernicus University, Grudziadzka 5, 87-100, Toruń, Poland
[c] Department of Experimental and Applied Physics, Faculty of Science and Technology, Jan Dlugosz University, Armii Krajowej 13/15, 42-200, Częstochowa, Poland
[d] Department of Rare Earths, Faculty of Chemistry, Adam Mickiewicz University, Uniwersytetu Poznańskiego 8, 61-614, Poznań, Poland
[e] AGH University of Krakow, Mickiewicza 30, 30-059, Krakow, Poland
[f] Institute of Nuclear Physics Polish Academy of Sciences, 31-342, Krakow, Poland
[g] BGE Bundesgesellschaft für Endlagerung mbH, Schachtweg 3, Ingersleben, OT Morsleben, 39343, Germany

ARTICLE INFO

*Keywords:*
Lyoluminescence
Blue halite
Sylvite
Luminescence dating
Colour centres
Morsleben

ABSTRACT

The potential of salt as an artificial and natural luminescence dosimeter is well documented in the literature. However, the potential of lyoluminescence, i.e., luminescence during salt dissolution, was neglected over time, and the first attempts to use LL as a natural dosimeter were not followed up on further. In this study, we build upon previous studies and investigate the LL properties of a sylvite vein containing blue halite from the salt repository Morsleben (Germany) and attempt to determine the timing of its last crystallization. We employed four experimental setups optimized for LL detection and present measurements using a high-sensitive CCD camera and photon counting heads to detect and prove the existence of natural LL signals in blue halite and sylvite. An enhanced LL signal was used to estimate the equivalent dose using an additive dose approach. Additional UV–VIS spectroscopy determined colour centres in the studied minerals towards a better understanding of the underlying LL mechanism. Our results indicate that the LL age underestimates the actual crystallization event of the old geological minerals in the repository due to long-term exposure to ionizing radiation. However, we are optimistic that the LL is a promising tool for dating the last crystallization event of certain minerals for younger repositories, where the exposure time was shorter.

## 1. Introduction

The potential of sodium chloride as a natural dosimeter for dating was first recognized by Bailey and Adamiec [1] and Zhang et al. [2], who used optically stimulated luminescence (OSL, [3]). They proposed that the optical dating of halite reflects its most recent crystallization event, making it a valuable tool for establishing a crystallization chronology in arid environments. Gartia [4] reported the application of sodium chloride as a paleothermometer due to the correlation between thermoluminescence (TL peaks) and the thermal annealing of *F*-centres. In luminescence-based dosimetry, numerous OSL and TL studies have explored the applications of salts, particularly in emergency scenarios (e.g., Refs. [5–9]). Most research naturally focuses on TL and OSL methods as the equipment is available off-shelf. However, another option to explore salt luminescence is through luminescent phenomena, such as lyoluminescence (LL) or chemiluminescence (CL), which can be induced by dissolving the mineral in a suitable solvent. The potential of the LL method in medical dosimetry using, among others, pure sodium chloride has already been confirmed by, e.g., Atari and Ettinger [10]. Among alkali halides, NaCl is the chemical compound with the highest LL efficiency, eight times higher than KCl [11]. Recently, attention has been focused on gamma-irradiated doped synthetic salts dissolved in luminol solution, such as $Dy^{3+}$-activated $(K_{0.5}Na_{0.5})Cl$ [12] or KCl:Dy [13] in which low fading and relatively high LL signal saturation dose seem to render these materials promising for accidental dosimetry. Still, there is a lack of data on natural LL signals from geological samples such

* Corresponding author. Institute of Geography, Heidelberg University, Im Neuenheimer Feld 348, 69120, Heidelberg, Germany.
*E-mail address:* magdalena.biernacka@uni-heidelberg.de (M. Biernacka).

https://doi.org/10.1016/j.jlumin.2025.121088
Received 12 November 2024; Received in revised form 9 January 2025; Accepted 16 January 2025
Available online 27 January 2025

as halite (sodium chloride) or sylvite (potassium chloride) minerals. Such data is fascinating for investigating the potential of LL, supplementing methods using natural minerals, such as quartz or feldspar, in a vast range of possible applications of luminescence-based geochronology. Contrary to conventional luminescence dating techniques, the event of interest is not the last exposure to sunlight or heat but the last event of hydration/dissolution. Therefore, studies of natural LL signals from minerals that crystallized under specific conditions are valuable in geochronology, which, in a broader context, can be used to study past landscapes.

Halite collected from K-rich sylvite environments seems promising for LL studies due to its naturally high internal beta and gamma-dose rate contribution. Prolonged exposure to natural ionizing radiation in the environment from the last crystallization event and crystal growth under specific conditions (high pressure and temperature) are responsible for forming defects such as colour centres and colloid metal nanoparticles in the crystal lattice. This usually causes characteristics of violet to blue in such halite. Sonnenfeld [14] reviewed potential reasons for these natural colour effects and postulated that descending brines rapidly become saturated with sodium and chlorine, leaching, brecciation, and recrystallization of halites, preferentially displaces bromine ions from the crystal lattices and leaving platelets of metallic sodium in the lattice defects, which ultimately cause the blue discolouration of halite. Recently, Calas et al. [15] found that the blue colour can be attributed to metallic sodium nanoparticles (2.5–3 nm) causing a surface plasmon resonance effect. Despite the ongoing discussion, common ground seems that even light earth pressures (kPa) may be sufficient to yield blue discolouration in naturally irradiated salt and that the blue colour of natural salt has been attributed to exposure to gamma rays, for instance, from $^{40}$K present in the sylvite accompanying halite deposits [16]. In terms of occurrence, samples of blue and violet halite variations associated with potassium minerals are typical late Permian (Lopingian, ca. 260 Ma to ca. 252 Ma; https://stratigraphy.org, last access: 2025-01-27) salt formation and have been investigated mainly because of their interesting optical properties. Typical formations can be found in, e.g., Kłodawa, Poland [17–21] or Morsleben, Germany [22,23]. For the blue halite from Kłodawa, their colour centres have been identified as *F*, $R_1$ ($F_3$), $R_2$ ($F_3$), *M* ($F_2$) and plasmons [18] and with a complete bleaching of the thermal centres at ca. 400 °C [20]. According to Arun [22], changes in Raman band intensities in the transparent and blue halite from Morsleben following proton beam irradiation indicate their potential application in radiation monitoring.

Blue halite was suggested as a potentially interesting material for LL studies in 1973 [24]. However, apart from a brief recognition of an unsuccessful preliminary study by Göksu et al. [25], we are unaware of further studies on this subject. The principle of LL is similar to other luminescence techniques. The crystallization stage is the complete zeroing of the luminescence signal, and the dose accumulates due to increasing the concentration of radiation-induced defects, including colour centres, over time. Defect concentrations are determined as a function of the dose and the irradiation temperature [26]. Studies in the context of radioactive waste storage have pooled information about radiation-induced defect types and their behaviours observed in rock salt [27]. If a controlled dissolution of such a crystal-rich in radiation-induced defects occurs, a luminescence signal can be recorded that is at least proportional to the concentration of *F*-centres and, in best-case scenarios, to all trapped electrons in the crystal (all-electron type centres). The latter highlights the potential advantage of the LL method over the TL or OSL: as all charge carriers are released from the traps during the LL measurement, the dose reading is total. Furthermore, the lack of residual signal in LL is a potential advantage, while naturally occurring inhomogeneity may add a different level of complexity.

This study presents the results of LL experiments of blue halite and sylvite collected from a sylvite vein rich in $^{40}$K in Morsleben (Germany). The aim is to assess whether a correlation between natural LL and the minerals' last crystallization event can be established, which may enable the calibration of this signal and its application as a new geochronological tool for application in Earth sciences. Using four experimental setups, we will first explore the optimal experimental conditions for LL on chloride minerals. We then report the readings of natural LL using photon counting heads and a high-sensitivity CCD camera setup, which also enables us to visualize, for the first time, the ultra-weak LL signals from the selected chloride minerals. The remainder will determine the equivalent dose for both minerals using the enhanced LL signals and determine age in combination with the effective dose rate. UV–VIS spectroscopy was employed to determine the colour centres in the investigated minerals, providing further insights into the LL mechanism. We will show that LL from natural minerals, enhanced with appropriate activators, may offer an additional luminescence dating tool for routine use in geochronology targeting the last recrystallization event.

### 1.1. LL theory and mechanisms

The common understanding of LL involves light emission by a previously irradiated crystal during its dissolution in a particular solvent. In inorganic materials such as alkali halides, LL is linked to crystal lattice defects called *F*-centres (the anion vacancy with captured electrons). Although the colour centres in alkali halides can be generated in various ways, only irradiation produces equal quantities of trapped electron-hole pairs in the crystal lattice. The LL was observed in additively coloured alkali halides [28,29]; however, it was found that the presence of both electron and hole-type centres is crucial for the manifestation of LL, as no centre alone can induce this phenomenon when pure water is used as a solvent.

In the simplified understanding of the LL mechanism (Eq. (1) and (2)) proposed by Atari in 1980, an alkali halide crystal releases a hydrated electron ($e^-_{aq}$) from an *F*-centre while in contact with a solvent (water). The rapid recombination of the hydrated electron, primarily with a $V_2$-center,[1] at the water-solid interface results in light emission, known as lyoluminescence. Hydrated electrons play a crucial role because they have a strongly reducing nature and react with oppositely charged particles on a nanosecond timescale in the solid-liquid interface, leading to light emission (LL) or exciting radicals in the solution that emit light upon returning to their ground state (CL):

$$F - centre \xrightarrow{hydration} e^-_{aq} \tag{1}$$

$$e^-_{aq} + V_2 \xrightarrow{recombination} h\nu \tag{2}$$

According to Arnikar et al. [30,31], the following chemical reactions can describe LL of a salt dissolving in pure water.

1) Release of hydrated electrons from the surface of crystals:

$$e^- + H_2O \rightarrow e^-_{aq} \tag{3}$$

2) The reaction of these electrons with hole centres on the crystal surface, excitation of chlorine atoms and LL emission with poor light efficiency:

$$e^-_{aq} + Cl^{\bullet}\, H_2O \rightarrow \left(Cl^-_{aq}\right)^* \rightarrow Cl^-_{aq} + h\nu \tag{4}$$

3) The side reaction of hydrated electrons with water molecules:

$$e^-_{aq} + e^-_{aq} + 2H_2O \rightarrow H_2 + 2OH^- \tag{5}$$

[1] The V2-center in NaCl is probably a $Cl_3^-$ quasi-molecule orientated along the <100> axis and occupying two anion sites and one cation site (cf. review of [27]).

The probability that reaction (5) occurs is on the order of $10^{-3}$; therefore, theoretically, it can be neglected in the balance of the consumption of hydrated electrons to generate LL photons. The low light production efficiency of LL in pure water is problematic, especially for LL signals from natural minerals. However, this efficiency can be controlled because the intensity of LL is influenced by several factors, including particle size and mass of the solute, pH value, temperature, volume and $O_2$ concentration of the solvent, absorbed dose, the density of the colour centres, type and concentration of impurities present, rate and time of dissolution, e.g., Refs. [32–34]. One of the most significant factors affecting luminescence intensity is the presence of chemical compounds that can enhance (activators, e.g., $Tl^+$, $Cu^{2+}$, luminol and fluorescence dyes), or quench (hydrated electron scavengers, e.g., $NO_3^-$, $CrO_4^-$, $MnO_4^-$ and $Cd^{2+}$ or $Zn^{2+}$) the emission efficiency. In the case that a salt solvent contains divalent copper ($Cu^{2+}$) as activators, the simplified LL mechanism, according to Atari [29] becomes:

$$F - centre \xrightarrow{hydration} e_{aq}^- \tag{6}$$

$$e_{aq}^- + Cu^{++} \xrightarrow{recombination} |Cu^+|^* \rightarrow Cu^+ + h\nu \tag{7}$$

Kalkar and Ramani [35] proposed the following reactions as the source of LL when divalent copper ions are present in solution:

$$\left([Cu(H_2O)_6]^{2+} + e_{aq}^- \rightarrow ([Cu(H_2O)_6]^+)^*\right) \tag{8}$$

$$([Cu(H_2O)_6]^+)^* \rightarrow [Cu(H_2O)_6]^+ + h\nu \tag{9}$$

$$[Cu(H_2O)_6]^+ + Cl^\bullet \rightarrow [Cu(H_2O)_6]^{2+} + Cl^- \tag{10}$$

According to Kalkar and Ramani [35], hydrated electrons in the solution reduce the complexed copper ion from oxidation state +2 to +1 (Eq. (8)). They also proposed excitation and emission of copper in the +1 oxidation state (Eq. (9)). However, it has been proved incorrect because chemiluminescence always occurs with the oxidation of Cu(I) to Cu(II). Therefore, we suggest the correction of the above reactions (see Sec. 3.4.1).

The general LL mechanism concerns the 'ideal' situation in which one type of electron centre (the *F*-centre) is present in the crystal, and it is assumed that a hole centre (most likely $V_2$) is also present when dissolution takes place in pure water (Eqs. (1)–(4)). However, if *F*-centre aggregates occur in the crystal, such as *M* or *R*, typical of blue halite variants (see Refs. [18–20], it should be taken into account that not all electrons released from the centres contribute to the LL radiative emission. From the work of Arnikar et al. [36], it follows that mainly the hydrated electrons originating from *F*-centres contribute to the LL signal, while the electrons released from *M*-centres can react with water differently to form dimers or pairs of hydrated electrons, causing an increase in the side reaction frequency (Eq. (5)).

To describe LL phenomenologically, Chandra et al. [37] proposed the following LL glow curve:

$$I = \frac{\eta\beta\gamma\alpha n_F N_0}{(\beta - \alpha)}\{exp(-\alpha t) - exp(-\beta t)\}; \quad \beta = \sigma_r N_r \upsilon, \tag{11}$$

where $\eta$ [−] is the radiative recombination probability, $\beta$ [$s^{-1}$] is the recombination rate constant of hydrated electron-hole pairs ($\sigma_r$ [$cm^2$] is the capture cross-section of holes, $N_r$ [$cm^{-3}$] is the density of recombination centres, i.e., holes, $\upsilon$ is [$cm{\cdot}s^{-1}$] the average velocity of the hydrated electrons), $\gamma$ [−] is the factor correlating the number of hydrated electrons and the number of dissolved *F*-centres, $\alpha$ [s] is the rate of dissolution of solute in the solvent, $n_F$ [−] is the density of *F*-centres, $N_0$ is the initial number of the molecules of a solute, and $t$ [s] is the time of dissolution.

Dissolving a solute in a solvent is slower than the recombination process of hydrated electrons with holes. Therefore, the assumption $\beta \gg \alpha$ can be made. For higher values of $t$, Eq. (11) changes to:

$$I = \eta\gamma\alpha n_F N_0\, exp(-\alpha t) \tag{12}$$

The equation shows that the LL intensity decreases exponentially with time. The total LL intensity, i.e., the total area below the LL intensity versus time, is directly proportional to the density of *F*-centres ($n_F$) and the initial number of the molecules of a solute ($N_0$) [37]. According to Dhoble et al. [38], the LL intensity depends on the concentration of colour centres and dissolution rate simultaneously.

However, it should be noted that a single-exponential decay kinetics is rarely observed in real LL signals. Banerji et al. [39] showed that the LL decay measured for gamma-irradiated NaCl, KBr and KCl dissolved in water exhibit a fast decay component with times of 0.5 s, 0.4 s, 0.2 s and a slow component, with times of 7.5 s, 4.3 s, 2.3 s, respectively. The decay kinetics seems independent of the absorbed dose in the 0.1–2 kGy range but depends on the dissolved material type [40].

## 2. Study site and sampling design

For our study, we collected samples from the Morsleben repository managed by the Bundesgesellschaft für Endlagerung (BGE). The salt formation at Morsleben, located in Saxony-Anhalt, Germany, is part of the North German Basin, belonging to the Zechstein Evaporite Series (Late Permian, ca. 259 Ma to 251 Ma; https://stratigraphy.org; last access: 2025-01-27). It contains rock salt, potassium-magnesium salts, and sulphates structured in diapirs, pillows, and walls [41]. Seven distinct cycles of the Zechstein formation (from Na1 to Na7) were identified due to alternating marine transgressions and regressions. The sampling site, shown in Fig. 1a), was located in segment 15YER21/R015 on the eastern flank of the first northern directional section (15YER21/R001) at 326 m below sea level. This part contains a sylvite vein with inclusions of blue halite, formed as secondary salt probably about 28 Ma ago (Oligocene). Although this site has not yet been dated, we assume that the formation time of this vein is consistent with the age assigned to polyhalite ($K_2Ca_2Mg(SO_4)_4{\cdot}2H_2O$) from Morsleben, which is 28.68 ± 0.11 Ma using the $^{40}Ar/^{39}Ar$ dating [42] and 28.2 ± 0.3 Ma using K-Ar dating (unpublished report). The vein is located in rock salt formed during the Z3 Leine Salt (Z3Na) cyclothem approximately 250 Ma ago. We core-drilled samples from two locations, depicted as Spot 1 and Spot 2 in Fig. 1a) (diameter: 11 cm; length ca. 7 cm), under subdued light conditions and stored them in opaque containers. We also retained the drill cuttings, mixed Spot 1 (**mS1**) and mixed Spot 2 (**mS2**), consisting mainly of sylvite. The blue halite was later separated from white sylvite (see Fig. 1b) in the luminescence laboratory under red light conditions. Samples containing blue halite were labelled as blue halite Spot 1 (**bhS1**) and blue halite Spot 2 (**bhS2**), while those containing sylvite were labelled sylvite Spot 1 (**sS1**) and sylvite Spot 2 (**sS2**), respectively. Separated samples of blue halite observed under daylight conditions exhibited varying intensities of blue colour saturation, unevenly distributed across the crystals (Fig. 1c). These crystals displayed regions with varying shades of blue, pale blue, or light purple, alternating with colourless sections. Moreover, the crystals of this blue halite did not develop idiomorphically, as indicated by the rounded edges of halite-containing areas and irregular shapes of halite that do not resemble a cubic structure. A detailed description of sample preparation can be found in Sec. 3.5. In some experiments, NaCl and KCl analytical-grade reagents were used as reference material.

## 3. Experimental

### 3.1. Instrumentation

Due to the lack of commercially available LL equipment, we used three systems to conduct our experiments. Two of the systems (Heidelberg University: UHD and Jan Dlugosz University: JDU) were dedicated to LL measurements for heterogeneous systems (solid and solution),

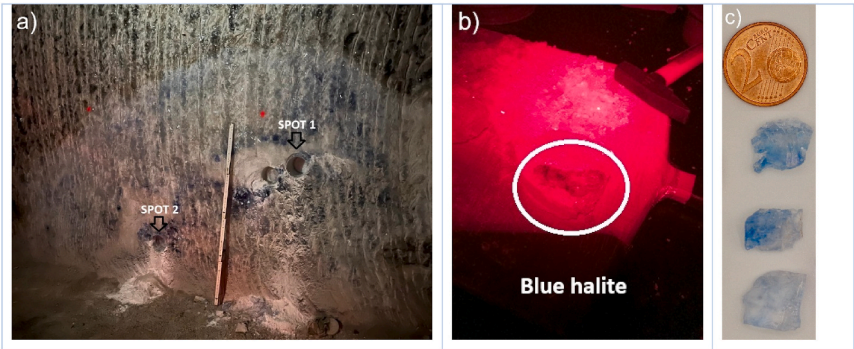


**Fig. 1.** Naturally discoloured aggregates of the blue halite surrounded by white sylvite; Morsleben repository (BGE), Saxony-Anhalt, Germany; a) sampling spots labelled with Spot 1 and Spot 2; b) part of the core from Spot 1 contain blue halite aggregation, c) samples of bhS1 exposed to daylight. (For interpretation of the references to colour in this figure legend, the reader is referred to the Web version of this article.)

while one (Adam Mickiewicz University: UAM) was initially designed for the chemiluminescence measurements in homogeneous systems (solutions only). All devices use photomultiplier tubes operating in photon-counting mode. They differ in geometry, size of the measurement chamber, solvent dosing methods, and software used. Different LL experiments were performed using various systems. A susceptible CCD camera-based optical detection system (Institute of Nuclear Physics Polish Academy of Sciences: IFJ PAN) was constructed to visualize the ultra-week natural LL signal. The detection range for all systems was chosen to cover LL emission wavelengths expected between 400 nm and 600 nm (e.g., Refs. [28,43]) and analogous to TL emission from these salts (e.g., Ref. [31]).

*3.1.1. Prototype LL reader (UHD)*

At Heidelberg, we designed and prototyped a portable LL system. Parts were printed with a MakerBot Method X Carbon Fibre Edition 3D FDM (fused deposited modelling) printer for rapid prototyping with polylactic acid (PLA) and acrylonitrile butadiene styrene (ABS). The LL system consists of a modular system for detection, sample chamber, and solvent injection. For detection, we employed an ET Enterprise model PDMF9107-USB-01 photomultiplier tube (PMT) operating between 280 nm and 630 nm without additional optical filters on detection. The PMT operates in continuous counting mode using software delivered by ET Enterprise and is connected via a USB-A connector. The solvent was injected into the LL system using an Aladdin programmable peristaltic pump, model AL-9000G (World Precision Instruments), from the start of signal recording, and the LL signal was integrated over 1 s per channel.

*3.1.2. LL system based on Helios reader (JDU)*

The LL measurements at JDU were performed using modified equipment based on the Helios reader series (Zero-Rad; http://zero-rad.com/; last access: 2025-01-27). This modular system can be used for LL and optically stimulated luminescence (OSL) measurements. It contains stimulation and detection modules enclosed in a light-tight aluminium housing. The device has a changeable chamber for a sample with or without a solvent transmitter. Detection is facilitated by a Hamamatsu PMT model H11870-01, detecting between 200 nm and 650 nm (peak sensitivity wavelength at 375 nm) without additional optical filters on detection. The PMT worked in counting photons mode and was protected by an ultra-thin electronic shutter (Melles Griot). No additional material stimulation (except the dissolution) was performed. The solvent was injected into the LL system using an automatic pipette at a set time from the start of the signal recording. The measurement was performed for 40 s, with a sampling channel resolution of 1 s per channel.

*3.1.3. Chemiluminescence system (UAM)*

We used equipment available at the Department of Rare Earths, Faculty of Chemistry, Adam Mickiewicz University (UAM) for recording ultra-weak LL emissions. A lightproof box contains an optical channel and a counting chart Advantech PCI-1780U, linked to a PC unit's main board. Software written in the Borland Delphi controls the setup. Luminescence generated in the process of LL was directed by the optical track and recorded using a M12FQC51 PMT operating in the spectral range 190–800 nm (peak sensitivity wavelength at 480 nm) in a single photon counting method in combination preamplifier, constructed based on a fast-operational amplifier ADA4817. To obtain the optimum signal-to-noise ratio, the signal was transformed by a comparator and regulated voltage discriminator and the TTL pulses obtained, additionally amplified by a Hamamatsu amplifier C5594-34, recorded by a PC via a chart Advantech PCI-1780U [44,45]. The optical track was calibrated by employing the standard CL reaction with 5-aminophthalic acid (luminol) and hydrogen peroxide in a DMSO solution. In these conditions, 1 $cm^3$ of luminol solution emits $(9.7 \pm 0.3)\bullet 10^{14}$ photons in the oxidation process [46]. The measurements were performed with a sampling time of 0.1 s per channel.

*3.1.4. The optical detection system for imaging of LL (IFJ-PAN)*

LL imaging was performed using a new configuration of the self-developed prototype optical detection setup, previously applied for the two-dimensional (2D) proton dose measurements [47]. For our study, the system has been specially adapted for imaging high-resolution LL signals. The investigated samples in the form of powder have been placed inside a Teflon-made cup with a hole for a needle, enabling simultaneous solvent (copper chloride or water) injection while recording LL signals. The system consists of an ANDOR iXon Ultra 888 back-illuminated EM-CCD camera with a Navitar 17 mm F/0.95 lens for image acquisition (see Fig. 2). The following camera parameters were adjusted in order to improve signal-to-noise ratios: CCD camera sensor cooled down to –81 °C, imaging area set to 512 × 512 pixels (16-bit format), pixel size 13 × 13 μm, electron multiplication (EM) gain set to 100 and pixel binning to 2 × 2. According to the manufacturer data, the quantum efficiency in the analysed sample's emission spectra range (approx. 500 nm) is up to 85 %. The camera setting enables the readout of a sample area with a maximum diameter of up to 45 mm. Images were acquired without filters between the lens and the samples using the *μManager* and *ImageJ* [48]. Images were captured in subdued light conditions with an acquisition time of 30 s, under a controlled injection solution. To calculate the signal level quantitatively, the following procedure was applied and repeated to each analysed chloride. First, a background image of the investigated sample was taken. Next, for the same natural or irradiated sample, an image under the controlled solvent (copper chloride solution or HLPC water) injection has been acquired. Finally, all captured LL images (after background subtraction) were further analysed as a sum value from an active sample area

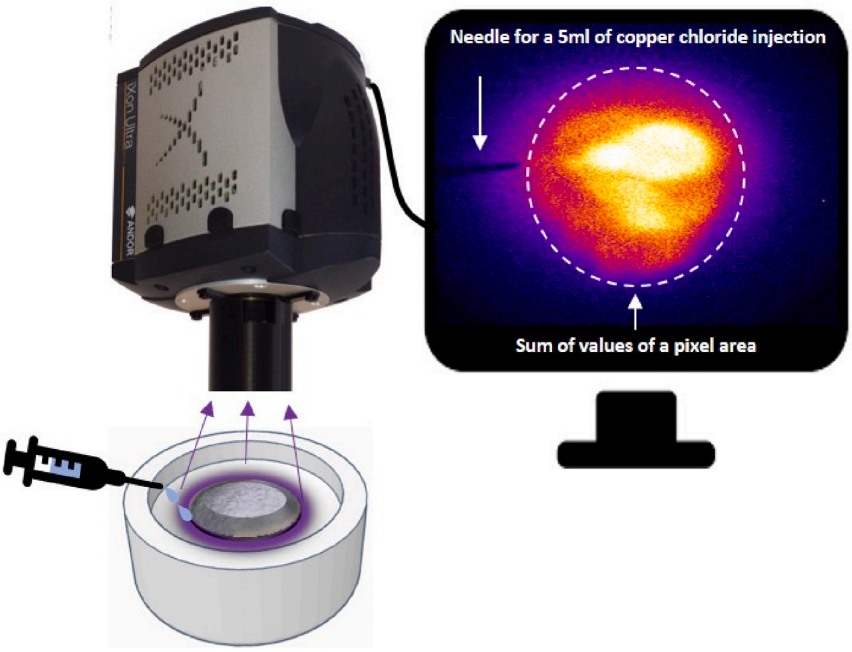


**Fig. 2.** Sketch of the prototype optical setup spatially resolved LL measurements. The setup consists of an ANDOR iXon Ultra 888 EM-CCD camera equipped with the Navitar 17 mm F/0.95 lens, a Teflon-made cup for the analysed halite sample and a hole for a needle used for copper chloride or water injection. The screen shows an example (https://www.geog.uni-heidelberg.de/geomorph/lyoluminescence.html; last access: 2025-01-27) of the acquired LL from one sample obtained using the *μManager* and *ImageJ* open-source software. The white dashed circle represents the active pixel area of a 300-pixel radius, taken during the analysing process of each retrieved LL image.

comprised of approx. 300 pixels central radius (see Fig. 2).

### 3.2. Dose rate determination

To quantify the radionuclides' ($^{40}$K, $^{235}$U, $^{238}$U, $^{232}$Th) concentration at our sample sites and estimate the effective dose rate, we employed three μDose [49,50] and one μDose+ system [51] in Heidelberg (devices: uDose_005P, uDose_025, uDose_027) and in Częstochowa (device: uDose_038). The effective dose rates were calculated with the μRate software v2022.5 (https://miu-rate.polsl.pl; last access: 2025-01-27) [52]. The μDose systems facilitate scintillator-based counting systems registering alpha and beta particles that are distinguished by their characteristic pulse shapes [53]. Radionuclides are separated based on typical decay pulse distributions used to classify decay pairs. All systems were re-calibrated prior to the measurement. To convert radionuclide concentrations to dose rates, we applied the conversion factors of Cresswell et al. [54]. For each spot (Spot 1 and Spot 2), we measured three different samples: a mixed component (mS1, mS2), sylvite (sS1, sS2), and blue halite (bhS1, bhS2). The preparation of the samples involved sieving to obtain the fraction <63 μm and drying at 50 °C for a couple of days just until the measurement to avoid moisture absorption of the salt prior to the measurements. We prepared 3 g (±0.1 %) of each sample immediately after removal from the drying oven. Measurement durations varied with the available machine time, but we aimed at a minimum of 1.5 days per sample to ensure suitable counting statistics. For comparison, the mixed component (mS1, mS2) was sent to the Archéosciences Bordeaux (France) laboratory for HPGe low-background gamma-ray spectrometry [55] on ca. 90 g of each sample (device: Prisna).

### 3.3. UV–VIS spectroscopy

The appearance of characteristic absorption bands in irradiated alkali halides has been studied in the past (e.g., Ref. [56]). For pure NaCl, investigated at room temperature, several absorption bands associated with trapped-electron centres were identified, i.e., $F$ (458 nm), $R_1$ (545 nm), $R_2$ (596 nm), $M$ (725 nm), and with trapped-hole centres, i.e., $V_2$ (223 nm) and $V_3$ (210 nm) [57]. For mineral samples such as blue halite from Kłodawa, the existence of $F$, $R_1$, $R_2$, and $M$ bands was confirmed by Zelek et al. [20], who also found unidentified and plasmon bands. Given the shared origin of blue Zechstein salts, we expected to observe comparable absorption bands in blue halite from Morsleben. We used UV–VIS absorption studies of blue halite samples to determine the presence of individual colour centre bands and correlate them with the natural LL emission. Sylvite was omitted in this study because we observed an ultra-weak natural LL signal only for this mineral (see Sec. 4.2).

For the UV–VIS measurements on blue halite from samples of Spot 1 and Spot 2, we employed a GemmoSphere™ spectrometer operating between 350 nm and 1000 nm. In this device, unpolished samples of a few millimetres in size were placed within an integrating sphere, reducing scattering effects caused by surface irregularities. Although the device is optimized for gemmology samples, it provided reliable data for general absorbance analysis of small, irregularly shaped solid samples. The experimental spectra were decomposed using the peak positions of components assigned according to the literature (see Ref. [58]). The shape of each peak was then fitted using a Lorentzian-Gaussian model with baseline correction. Finally, the sum of all calculated peak components was pooled to compare the calculated spectra model with the experimental data.

The $N$, i.e., the number of each colour centre population per unit volume [cm$^{-3}$] (henceforth referred to as centre concentration), was calculated according to the Smakula [59] equation tested experimentally by Seinen et al. [26]:

$$N = 1.18 \bullet 10^{16} \bullet k_m \bullet W_{1/2} \quad (13)$$

where $k_m$ [cm$^{-1}$] is the maximum absorption constant; $W_{1/2}$ [eV] is the full width of the absorption band at half-maximum.

We identified characteristics of absorption bands associated with the presence of colour centres in blue halite from Morsleben, similar to earlier observations for those from Kłodawa [18,20].

### 3.4. Optimization of the LL readout

To optimise the measurement conditions, we had to optimise various experimental parameters. These parameters and the chosen settings will be detailed in the following to foster transparency and experimental reproducibility.

#### 3.4.1. Solvent type and activator

Initially, highly pure water (HPLC) was used for dissolution. However, a reaction activator was used due to the poor emission efficiency. Copper ions were chosen to enhance the LL signal because they are advantageous over thallium ions in terms of handling safety, do not exhibit photoluminescence, provide a stable background during measurements, unlike luminol, and do not significantly shift the LL emission spectrum as is the case for fluorescein or eosin. At the same time, it ensures the best among other transition metal ions $Mn^{2+}$, $Fe^{2+}$, $Co^{2+}$ and $Ni^{2+}$ amplification of LL emission [60]. Due to the lack of consistency in the literature data regarding the optimal concentration of copper ions for the enhancement of LL signals from laboratory-irradiated sodium and potassium chlorides (e.g., $5{\cdot}10^{-3}$ mol dm$^{-3}$ [29], $3{\cdot}10^{-4}$ mol dm$^{-3}$ [35] and $2{\cdot}10^{-4}$ mol dm$^{-3}$ [60]) in this work, the optimal concentration was established in the UAM system at $5{\cdot}10^{-4}$ mol dm$^{-3}$ for sample bhS1 (see Fig. S1). Moreover, we observed that copper cations, forming complex compounds with chloride ions in an aqueous solution, have significantly accelerated the dissolution process of tested salt samples. Therefore, we propose the following LL mechanism describing the emission during the dissolution of naturally irradiated salts in copper chloride solution.

After liberation and hydration of electrons, according to Eq. (3), the copper is reduced from oxidation state +2 to +1 by $e^-_{aq}$ with the formation of a copper-chlorine complex in the coordination zone:

$$[Cu(H_2O)_6]^{2+} + e^-_{aq} \rightarrow [Cu(H_2O)_6]^{+} \quad (14)$$

Excitation of copper by oxidizing it to +2:

$$[Cu(H_2O)_6]^{+} + Cl \rightarrow ([CuCl(H_2O)_5]^{+})^{*} + H_2O \quad (15)$$

Radiation deactivation of copper complex and LL light emission:

$$([CuCl(H_2O)_5]^{+})^{*} \rightarrow [CuCl(H_2O)_5]^{+} + h\nu \text{ (high light efficiency)} \quad (16)$$

Using a copper chloride solution of this concentration, we obtained an enhancement of the natural LL signal compared to water HLPC of an average of 13 folds for the bhS samples using all systems, whereas no significant enhancement was observed for sS samples. The enhancement rate for laboratory irradiated samples was similar for the bhS sample (13 folds) and noticeable (5–6 folds) for the sS sample.

#### 3.4.2. Solvent volume, temperature, and oxygen content

The solvent volume used was experimentally optimized and set to 5 ml, except for the JDU Helios reader, which was reduced to 0.5 ml due to the limited volume of the sample chamber. Despite experimental evidence in the literature (e.g., Ref. [32]) reporting a temperature increase of LL from salts dissolved in pure water by up to three times as the temperature rises (20 °C and 60 °C), we decided to conduct LL measurements at room temperature (21 °C–27 °C) to ease the experimental design and compare results between measurement systems. The quenching effect of molecular oxygen on LL is known when irradiated salt is dissolved in water solutions (e.g., Ref. [61]). However, we did not observe any significant effect on the oxygen concentration in the natural LL signal from bhS1 dissolved in copper chloride solvent (see Fig. S2).

#### 3.4.3. Solute mass and particle size

Initially, measurements were conducted on max. 100 mg thin slices cut from samples with millimetre-sized edges. This approach aimed to avoid triboluminescence, which caused the loss of natural LL [62] and prevented the generation of biasing recombination centres on the crystal surface due to mechanical stress. Unfortunately, it was impossible to record a measurable and repeatable natural LL signal for any sample prepared in this way at UHD and UAM, so we opted for the preparation procedure I, outlined in Sec. 3.5.

The optimal crystalline particle size suggested earlier for sodium chloride was around 80 μm [63], we preferred the fraction 125–212 μm in this work for the following reasons: i) the differences in LL intensity for particles between 90 μm and 315 μm are small (see Fig. S3); ii) the colour behaviour is well-visible of crystalline particles in this range, as for smaller particles, each sample became white; iii) the source calibration at UHD was based on quartz grains of similar range.

The dependence of LL on the sample mass has been studied many times so far (e.g., Ref. [64]), and it has been observed that the LL signal saturates with the mass of the dissolved salt, which depends on the total number of colour centres produced and the solubility of each salt. In this study, the sample mass was experimentally optimized, around 30 mg, while for the JDU system, it was 1–2 mg due to the limited capacity of the measurement chamber.

#### 3.4.4. Impact of visible light on the bleaching of the natural LL signal (photo-annealing effect)

Arnikar et al. [65] found that the energy barrier required to mobilize electrons involved in LL is around 1.11 eV for NaCl and 0.16 eV for KCl. Therefore, we investigated the impact of exposure to sunlight and standard fluorescent lighting under laboratory conditions on the natural LL signal of sample bhS1. We found only a negligible reduction in the natural LL signal compared to samples stored in darkness since their extraction from the mine, given the careful handling of the samples. After prolonged exposure to intense light for 6 h, we recorded a reduction of natural LL signal in blue halite of about 25 %, which is within the accepted statistical error of LL measurements (see Fig. S4). On the contrary, no quantifiable changes were observed for shorter exposure times on the order of a few minutes. This may be attributed to the fact that the relative number of centres with different stabilities depends significantly on the conditions under which they were formed [66]. Therefore, the natural LL was measured under reduced ambient light rather than in complete darkness, which simplified the experiments and enabled precise control of the sample mass, as the precision in determining the sample mass had a more significant effect on the reproducibility of the LL results than short-term exposure of the natural sample to external light.

#### 3.4.5. Laboratory irradiation and storage conditions

Due to the thermally stimulated recombination of electrons with *V*-centres, freshly irradiated NaCl crystals exhibit room-temperature luminescence (RTL), which decays exponentially at room temperature [67]. To achieve reproducible LL intensity, it is recommended that the RTL depletes before measurements [33]. In our experiments, we irradiated samples with a $^{90}Sr/^{90}Y$ beta source at room temperature, with varying beta-dose rates depending on the setup: 873 Gy h$^{-1}$ at UHD, 45 mGy h$^{-1}$ at JDU, and 192 Gy h$^{-1}$ at IFJ-PAN. After irradiation, the samples were stored for a minimum of three days to minimize the contribution of the RTL signal. The samples were kept in darkness at room temperature throughout the irradiation process and during storage. No additional humidity protection was applied unless the storage period exceeded three days; in that case, the samples were stored in airtight containers. LL of the laboratory irradiated samples was recorded under red light due to the well-documented sensitivity of freshly generated *F*-centres to visible light (e.g., Ref. [68]).

### 3.5. Lyoluminescence sample preparation procedure

I Detailed LL sample preparation
1 Sample collection in the mine and protection from light and moisture
2 Separation of sylvite from halite in laboratory conditions under red light
3 Gentle grinding in a mortar to avoid loss of signal due to triboluminescence
4 Drying for at least 16 h at 50 °C
5 Sieving to isolate crystalline fractions
6 Sealing in hermetic, lightproof containers
7 Optional: Heating the samples to 400 °C at a controlled rate of 15 °C·min$^{-1}$ and allow them to cool naturally to room temperature
8 Optional: Irradiation of small portions taken from samples prepared in Step 6 or 7
II Measurement of the natural LL signal
1 Weighing the material from Step I.6 under reduced ambient lighting
2 Placing the material in a clean and dry measurement chamber
3 Dosing of solvent (HPLC water or copper chloride solution) with simultaneous light emission measurement

### 3.6. Dose-response measurements for equivalent dose estimation

The concentration of colour centres in alkali halide crystals is closely related to the absorbed radiation dose. Mador et al. [68] and Gordon and Nowick [69] demonstrated that the colour formation in these crystals occurs in two stages: an initial rapid phase where inherent vacancies are filled, followed by a slower phase in which vacancies created by ionizing radiation trap electrons to form *F*-centres. In the case of laboratory gamma-irradiated NaCl dissolved in pure water, the dose is measurable in the range of 0.01 Gy–10 kGy with an accuracy of 5 % [24], and the LL signal remains stable at 85 % within 7 months post-irradiation [10] when the material is stored in the dark. These results were consistent with earlier findings by Arnikar et al. [31]. The crystal purity, grain size, and thermal history (annealing) influence LL dose-response characteristics in salts. The background signal of LL emission from non-irradiated samples influences the lower dose threshold. This background is believed to result from spontaneously formed colour centres, defects caused by mechanical handlings and impurities within the crystal or solvent [32].

We measured the dose dependences for blue halite (bhS1, bhS2) and sylvite (sS2) prepared according to procedure I (see Sec. 3.5). Samples were divided into equal subsamples and then irradiated with various doses. The total dose was the sum of the natural and laboratory doses. The LL signals were summed and averaged, and the standard deviation of the mean expressed the uncertainties. Because samples cannot be recovered after measurement, we used the additive dose method to determine the equivalent dose ($D_e$) instead of the single-aliquot regenerative dose (SAR) protocol [70] suggested by Zhang et al. [2] for OSL dating of halite. The limitation of the additive dose method is that it does not account for residual signals in the material. However, we assume that the high temperature in the sylvite vein reset residual signals.

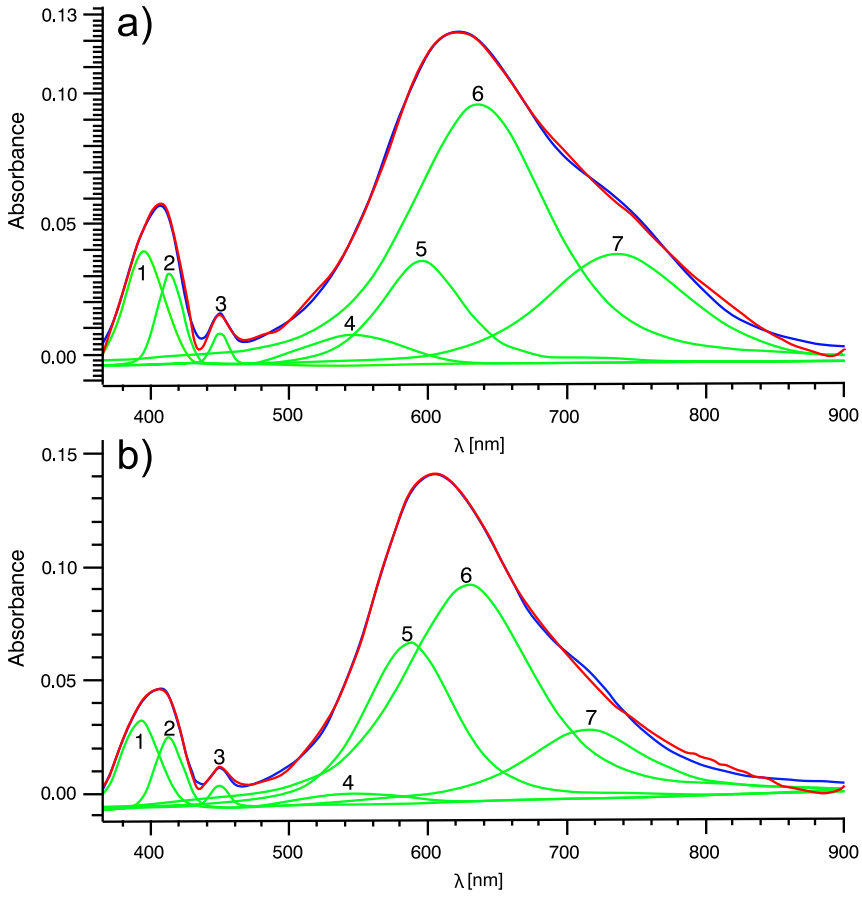


**Fig. 3.** a, b) Optical absorption spectra of studied crystals showing: *F*-centre, *F*-aggregates and plasmon bands for blue halite samples from Morsleben: (a) bhS1#2c; (b) bhS2#1f. (For interpretation of the references to colour in this figure legend, the reader is referred to the Web version of this article.)

## 4. Results

### 4.1. Material characterisation - UV–VIS spectroscopy

Examples of the obtained UV–VIS results are shown in Fig. 3 a), b), and all data are listed in Table 1. We identified seven absorption bands, most of which we could correlate with known colour centres in NaCl discoloured by long-term exposure to ionizing radiation. The far-UV region was outside the equipment's spectral range, so we could not investigate the presence of $V_2$ and $V_3$ centres in the samples. We found two unidentified bands with maxima around 391 nm and 413 nm, which may relate to the *F*-band, whose absorption band maximum was around 450 nm. This position for the *F*-band is consistent with the positions of this band measured for synthetic NaCl at room temperature, such as 458 nm [58] and 465 nm [71]. Only in sample bhS1#3b, we could not detect the 450 nm band. However, in this sample, the positions of all other maxima slightly deviate from those in the other samples, and the reason for this is unclear. The natural LL signal in the blue halite samples from Spot 1 and Spot 2 was highly reproducible (see Fig. 4), and the variation between individual blue halite samples in the results presented in Table 1 is not considerable. Moreover, the appearance of the complex structure of the *F*-band and the existence of the unidentified band in the blue region are consistent with previous observations for blue halites from Kłodawa [20]. The aggregated bands $R_1$, $R_2$, and *M* occur in all the tested samples, and their positions are consistent with literature data (e.g., Refs. [57,58]). Similarly, the plasmon band associated with the occurrence of colloidal sodium, both due to its dominance in the absorption intensity and to the position of the band maximum and half-width, is consistent with previous observations for blue halite from Kłodawa [18,20]. As observed in the blue halite from Kłodawa, the presence of the plasmon band in the blue halite from Morsleben indicates the natural nanocomposite structure of the material, where sodium nanoparticles are distributed in the NaCl matrix. The estimated centre concentrations (using Eq. (13)) for each absorption band on the order of $10^{15}$–$10^{16}$ cm$^{-3}$ suggest a high population of colour centres in the blue halite from Morsleben, which is in line with previous observations for the blue halites from Kłodawa $10^{16}$–$10^{18}$ cm$^{-3}$, [18]).

### 4.2. LL signal measurements

Differences in the LL intensity emission of blue halite, sylvite, and mixtures of these materials were visualized using an optical detection setup described in Sec. 3.1.4 (see Fig. 2). These measurements were always conducted on at least three subsamples of each sample to validate the obtained images. Under identical measurement conditions, images of similar brightness and texture, characteristic of each sample, were observed. Qualitative differences in the LL emission intensity of the selected samples are illustrated by the images shown in Table 2. The blue halite samples (bhS) consistently exhibited the highest LL signal brightness and a uniform image of the luminescent area. This indicates a significant population of crystalline particles contributing to the LL signal in these samples. The second brightest LL emission was observed in the halite and sylvite mixtures with a predominance of sylvite (mS). In this case, bright spots and streaks on the images likely originated from the blue halite present in the sample. This becomes evident when comparing the images with those of 'pure' sylvite (sS). These samples showed the lowest natural LL emission, practically non-detectable by the camera and only minimal LL emission after exposure to a dose of 100 Gy. In the latter case, the sS sample images revealed that only a few crystalline particles emitted LL during dissolution. This suggests that it is not the sylvite itself but the natural inclusions of microcrystalline halite particles within the sylvite sample responsible for the LL emission. A confirmation requires mineralogical composition studies of the sylvite sample, which are beyond the scope of this study.

Natural LL signals were measured independently using the UHD, JDU, and UAM systems to verify our findings. Reproducibility of the

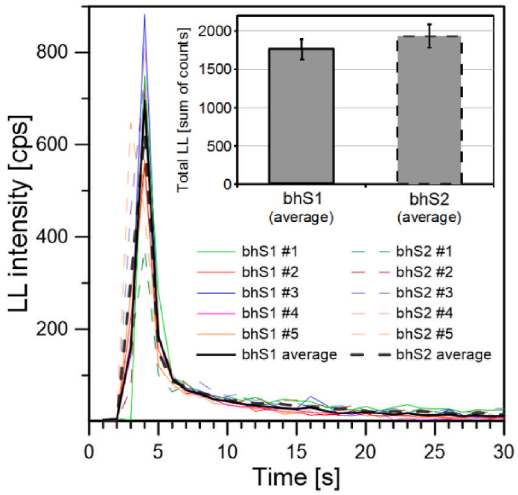


**Fig. 4.** Comparison of the natural LL intensity for blue halite samples from Spot 1 and Spot 2 measured using the JDU system. Inset: sum of counts over 0–40 s for average LL signals after background subtraction. Uncertainties represent the standard deviation of the mean. (For interpretation of the references to colour in this figure legend, the reader is referred to the Web version of this article.)

**Table 1**
Description of the UV–VIS absorption bands for blue halite samples from Morsleben collected from Spot 1 and 2.

| Sample Thickness [cm] | Experimental maxima of bands positions $\lambda_{max}$ [nm], $W_{1/2}$ [nm], *N* concentration [cm$^{-3}$] | | | | | | | |
|---|---|---|---|---|---|---|---|---|
| | | Unidentified band 1 | Unidentified band 2[a] | *F*-band | $R_1$ ($F_3$) band | $R_2$ ($F_3$) band | Plasmon band | *M* ($F_2$) band |
| bhS1#1a | $\lambda_{max}$ | 391 | 415 | 448 | 547 | 586 | 627 | 705 |
| 0.479 | $W_{1/2}$ | 37.0 | 22.3 | 10.2 | 80.0 | 64.0 | 86.8 | 100 |
| | *N* | 2.95E+16 | 2.31E+16 | 2.12E+16 | 5.90E+15 | 3.06E+16 | 3.52E+16 | 1.18E+16 |
| bhS1#2c | $\lambda_{max}$ | 394 | 413 | 449 | 547 | 595 | 636 | 737 |
| 0.515 | $W_{1/2}$ | 33.3 | 22.1 | 14.5 | 80.0 | 68.5 | 117 | 120 |
| | *N* | 3.79E+16 | 4.48E+16 | 2.52E+16 | 4.16E+15 | 1.65E+16 | 2.43E+16 | 9.98E+15 |
| bhS1#3b | $\lambda_{max}$ | 392 | 410 | – | 500 | 570 | 614 | 700 |
| 0.625 | $W_{1/2}$ | 32.5 | 20.5 | – | 60.0 | 100 | 103 | 60.0 |
| | *N* | 1.11E+16 | 8.46E+15 | – | 8.49E+15 | 2.47E+16 | 3.18E+16 | 5.26E+15 |
| bhS2#1e | $\lambda_{max}$ | 391 | 413 | 448 | 520 | 590 | 633 | 705 |
| 0.289 | $W_{1/2}$ | 32.0 | 23.1 | 8.79 | 70.0 | 74.9 | 84.8 | 100 |
| | *N* | 2.73E+16 | 2.47E+16 | 1.44E+16 | 8.21E+15 | 1.72E+16 | 3.48E+16 | 1.22E+16 |
| bhS2#1f | $\lambda_{max}$ | 392 | 413 | 449 | 547 | 587 | 629 | 715 |
| 0.282 | $W_{1/2}$ | 32.3 | 23.4 | 14.7 | 80.0 | 75.1 | 109 | 100 |
| | *N* | 6.51E+16 | 7.10E+16 | 3.52E+16 | 3.30E+15 | 4.93E+16 | 4.59E+16 | 1.61E+16 |

[a] Or also *F*-band.

**Table 2**
LL emission captured using an optical detection system (described in Sec. 3.1.4.) during the dissolution of natural and beta-irradiated powdered salt samples in pure water HLPC and copper chloride solution. Colours do not correspond to the wavelength of the light emitted during the experiment but were chosen for better visualisation.

| Sample | bhS | mS | sS | bhS | mS | sS |
|---|---|---|---|---|---|---|
| Solvent | Water HLPC | | | $CuCl_2$ solution | | |
| Nat. dose | 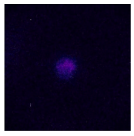 |  |  | 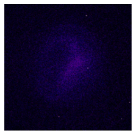 | 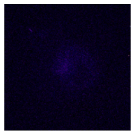 |  |
| Mass normalized LL intensity [arbitrary units] | 4.7E+04 | 3.3E+04 | 3.0E+04 | 1.0E+05 | 5.3E+04 | 2.4E+04 |
| Nat.+lab. 100 Gy dose[a] | 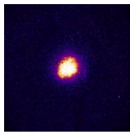 | 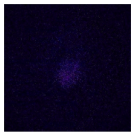 |  | 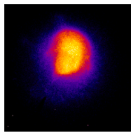 | 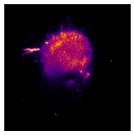 | 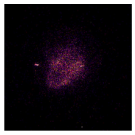 |
| Mass normalized LL intensity [arbitrary units] | 2.7E+05 | 5.6E+04 | 2.7E+04 | 3.4E+06 | 1.2E+06 | 1.7E+05 |

[a] Dose rate 192 Gy $h^{-1}$, storage time 96 h.

natural LL signal was achieved in multiple measurements, with similar results obtained for both sampling points, Spot 1 and Spot 2. The uncertainty in the total photon counts for the natural LL signals did not exceed 25 % and is caused mainly by the inhomogeneity of natural material, whereas the obtained reproducibility was achieved due to a well-controlled dissolution process. Fig. 4 presents typical high reproducible results of natural LL for blue halite samples in copper chloride solution with a concentration of $5{\cdot}10^{-4}$ mol $dm^{-3}$ measured using the JDU system. The total averaged LL signals for the blue halite samples from Spot 1 and Spot 2 did not differ significantly (see insert in Fig. 4). Therefore, we conclude that the sampling locations did not affect the obtained LL results. The kinetics of the LL decay curves were not analysed in this work. The natural LL signal for sylvite was indistinguishable from the PMT background level, and therefore, it was omitted from Fig. 4.

For comparative purposes, LL measurements were performed for pure, analytical-grade NaCl and KCl, both non-irradiated and beta-irradiated, using the JDU system. The background level from the copper chloride solution was also compared with the PMT background for the empty measurement setup. As expected, NaCl had significantly higher LL intensity than KCl, while no contribution to the LL emission from the copper chloride solution was detected (Fig. 5).

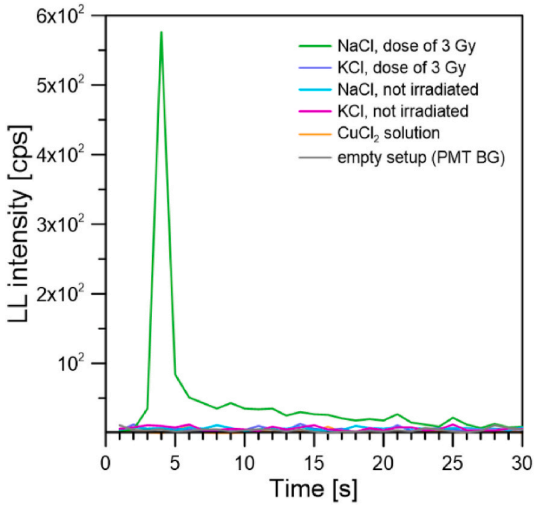


**Fig. 5.** Comparison of the LL signal intensity for non-irradiated and beta-irradiated analytical-grade NaCl and KCl measured using the JDU system.

### 4.3. *Thermal annealing and radiation-induced LL signal measurements*

As shown earlier (see Sec. 3.4.4), exposure to visible light does not significantly quench the natural LL signal in blue halite samples. Therefore, an attempt was made to quench this signal thermally in halite and sylvite samples. Zelek et al. [20] demonstrated that all colour centres in blue halite from Kłodawa disappear after annealing to 400 °C; hence, we repeated this experiment to eliminate the natural signal in the samples from Morsleben and measure the LL response to a laboratory dose. For LL signals measured five times for each sample type (bhS1, bhS2, sS2) after annealing at 400 °C, we recorded only photomultiplier background count rate, indicating complete zeroing of the natural dose. However, after irradiation, a similar decrease in LL signal sensitivity was observed for the blue halite samples, with reductions of 30.6 % and 29.2 % for bhS1 and bhS2, respectively (see the difference in bar height

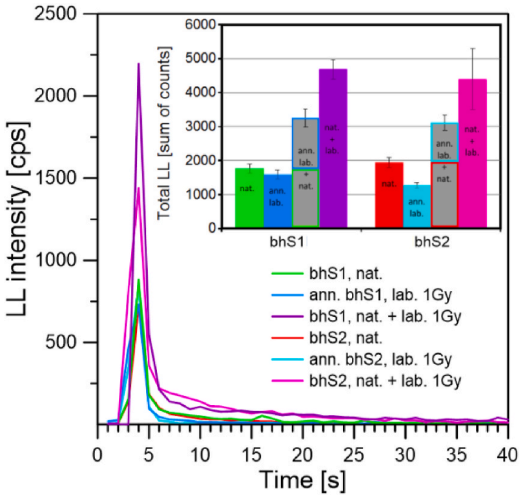


**Fig. 6.** Comparison of the LL signal for natural and irradiated halite measured using the JDU system. Inset: sum of LL counts over 0–40 s after background subtraction, uncertainties represent the standard deviation of the mean. Abbreviations: nat. - natural dose; ann. - annealing at 400 °C (removal of the natural signal), lab. - laboratory dose of 1 Gy; nat. + lab. - delivery of the laboratory dose to samples without removing the natural dose; nat. + ann. lab.

between 3 and 4 in the inset of Fig. 6), along with a significant increase in sensitivity of approximately 100 % for the annealed sylvite (sS2) sample (omitted from Fig. 6). Changes in the sensitivity of alkali halides in luminescence measurements after annealing have been observed earlier, for example, annealing of pure KCl at 400 °C leads to a significant increase of the OSL signal [72], which agrees with the observations for sylvite. The higher sensitivity can be explained by increased ion vacancies with annealing temperature and, hence, a higher corresponding colouration [73]. In future studies, EPR spectroscopy can provide additional insights into the concentration of anion vacancies, but this analysis falls outside the scope of the present study.

### 4.4. Dose-response curves and equivalent dose estimation

The results of LL measurements as a function of the laboratory dose are presented in Fig. 7 a) b) and Fig. 8. The function describing the growth of LL with dose was fitted to the measured values using the following function:

$$L = f(D) = L_0 + a_1 D + a_2\left(1 - e^{-a_3 D}\right) \quad (17)$$

where $L$ is the lyoluminescence intensity per Gy, $D$ is the absorbed dose in Gy, $a_1$, $a_2$, $a_3$ and $L_0$ are fitting parameters, with $L_0$ corresponding to the initial (natural) lyoluminescence per Gy.

In the simplest case, when dose dependence can be fitted with a linear function ($a_2 = 0$), Eq. (17) can be simplified as follows:

$$L = f(D) = L_0 + a_1 D \quad (18)$$

After fitting, these functions were extrapolated, yielding the $D_e$.

Fig. 7 compares the dose dependencies in the range of 0.03–10 Gy for samples bhS1 and bhS2 (a) and sS2 (b), measured for a storage time of three days between beta irradiation at a dose rate of 45 mGy h$^{-1}$ and the reading of LL in copper chloride solution using the JDU measuring system. Fig. 8 shows the result of the same sample bhS1 measured on the UHD measuring system using copper chloride solution at doses ranging from 1 Gy to 5,000 Gy, stored for 16 weeks in the dark after irradiation at a dose rate of 873 Gy h$^{-1}$. In this case, the integrated LL signal of each subsample was normalized to its mass, and the averaged values are shown in Fig. 8. In all graphs, the points represent the experimental average values of several subsamples and the uncertainties (standard deviation of the mean). The fit equations and the quality of the fits are given in the figure captions and legends. For each case, $D_e$ was determined together with uncertainty. The validation measurement shown in Fig. 8 was performed in a wide range of doses to check the correctness of the previously obtained result. Although consistent with each other, the $D_e$ results shown in Fig. 7 a) and b) indicate a much lower $D_e$ value than

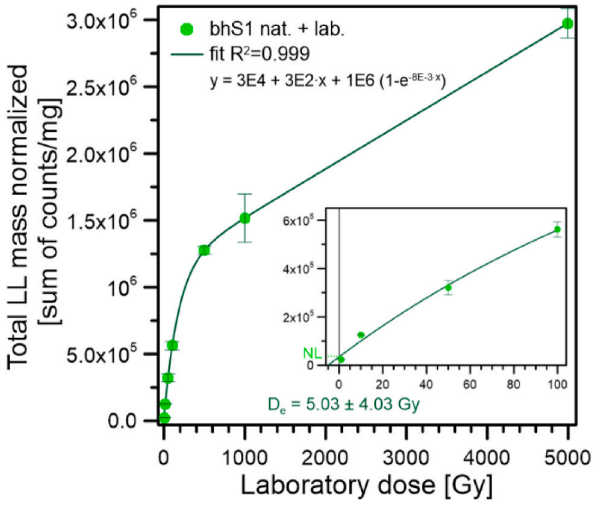


**Fig. 8.** Dose-response dependence using an additive dose approach was measured using the UHD system to determine the equivalent dose for the blue halite from Spot 1 (bhS1). Inset: the same data is shown for a limited dose range for better visualisation of $D_e$ estimation. (For interpretation of the references to colour in this figure legend, the reader is referred to the Web version of this article.)

we expected to obtain for these samples. However, the results obtained for a much wider range of doses, on a different measurement system, and for a much longer storage time of the samples (which was supposed to allow for observing fading in this sample as well) did not result in a significant difference in the determined $D_e$ value (see the inset of Fig. 8). Due to the consistency of the obtained results, age calculations were made in Sec. 4.6 based on the $D_e$ results shown in Fig. 7 a) and b). Nevertheless, an improvement in the reliability of the obtained $D_e$ will be necessary in future studies.

### 4.5. Effective dose rate results

We list the results of the radionuclides' measurements and the derived dose rates in Table 3. For the dose rates, we assumed a residual gravimetric water content of 1 ± 1 %. We obtained similar results for the mixed components of both spots and the three machines with central values [74] for $^{40}$K of ca. 44 ± 1 % (mS1) and 43 ± 1 % (mS2), and amounts of U and Th below the determination limit of our equipment. These results were confirmed by low-background gamma-ray

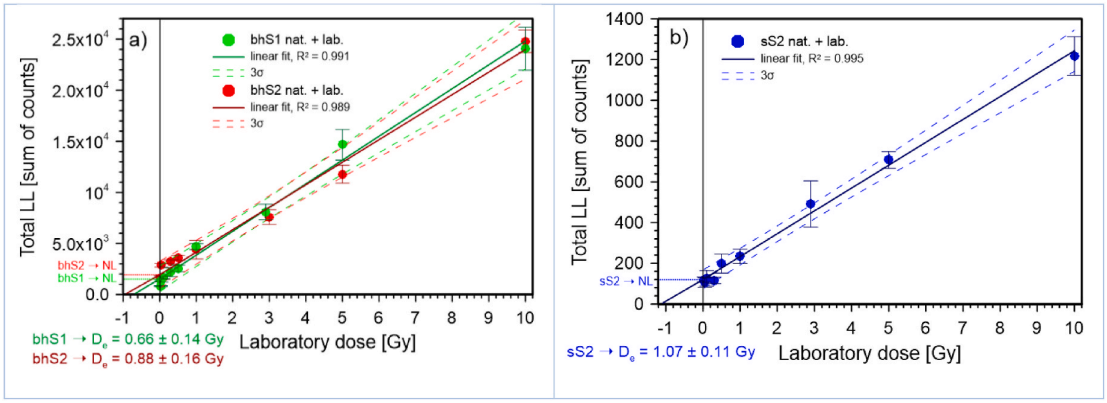


**Fig. 7.** Dose-response dependence and the additive method for determining the equivalent dose in (a) blue halites and (b) sylvite, measured using the JDU system. Function parameters read: blue halite Spot 1 (bhS1): $L = 2328\ D + 1537$; blue halite Spot 2 (bhS2): $L = 2204\ D + 1943$; sylvite Spot 2 (sS2) $L = 112\ D + 120$. (For interpretation of the references to colour in this figure legend, the reader is referred to the Web version of this article.)

**Table 3**
Radionuclide concentration results for the salt from Spot 1 and Spot 2 for the mixed (mS1, mS2), the sylvite (sS1, sS2) and the blue halite (bhS1, bhS2) samples. Uncertainties are quoted as the 68 % confidence interval. For U and Th, concentrations were below the determination limit in all cases and, therefore, considered negligible. All values are similar within 2-sigma uncertainties.

| # | DEVICE | $^{232}$Th | $^{238}$U | $^{235}$U | $^{40}$K | $\dot{D}_{beta}$ | $\dot{D}_{gamma}$ | $\dot{D}_{total}$ |
|---|---|---|---|---|---|---|---|---|
| | | [μg g$^{-1}$] | [μg g$^{-1}$] | [μg g$^{-1}$] | [%] | [Gy ka$^{-1}$] | [Gy ka$^{-1}$] | [Gy ka$^{-1}$] |
| mS1 | uDose_005P | <0.01 | <0.01 | <0.01 | 41.86 ± 0.43 | 35.4 ± 0.6 | 10.3 ± 0.2 | 45.7 ± 0.7 |
| mS1 | uDose_027 | <0.01 | <0.01 | <0.01 | 43.38 ± 0.47 | 36.8 ± 0.7 | 10.7 ± 0.2 | 47.6 ± 0.7 |
| mS1 | uDose_038 | <0.01 | <0.01 | <0.01 | 47.35 ± 0.51 | 40.1 ± 0.8 | 11.6 ± 0.2 | 51.7 ± 0.8 |
| mS2 | uDose_005P | <0.01 | <0.01 | <0.01 | 41.64 ± 0.43 | 35.2 ± 0.7 | 10.2 ± 0.2 | 45.5 ± 0.7 |
| mS2 | uDose_025 | <0.01 | <0.01 | <0.01 | 42.86 ± 0.46 | 36.8 ± 0.7 | 10.7 ± 0.2 | 47.6 ± 0.7 |
| mS2 | uDose_038 | <0.01 | <0.01 | <0.01 | 45.36 ± 0.49 | 38.4 ± 0.7 | 11.1 ± 0.2 | 49.5 ± 0.8 |
| bhS1 | uDose_038 | <0.01 | <0.01 | <0.01 | 8.35 ± 0.12 | 7.1 ± 0.15 | 2.1 ± 0.05 | 9.1 ± 0.2 |
| sS1 | uDose_038 | <0.01 | <0.01 | <0.01 | 53.80 ± 0.58 | 45.5 ± 0.9 | 13.2 ± 0.3 | 58.7 ± 0.9 |
| bhS2 | uDose_038 | <0.01 | <0.01 | <0.01 | 3.58 ± 0.07 | 3.04 ± 0.08 | 0.9 ± 0.02 | 3.9 ± 0.9 |
| sS2 | uDose_038 | <0.01 | <0.01 | <0.01 | 53.25 ± 0.57 | 45.5 ± 0.9 | 13.2 ± 0.3 | 58.1 ± 0.9 |
| mS1 | HPGe (Prisna) | <0.01 | <0.01 | <0.01 | 43.5 ± 0.4 | – | – | – |
| mS2 | HPGe (Prisna) | <0.01 | <0.01 | <0.01 | 42.3 ± 0.4 | – | – | – |
| Central value mS1 | | | | | 44.1 ± 1.3 | 37.4 ± 1.1 | 10.9 ± 0.3 | 48.3 ± 1.4 |
| Central value mS2 | | | | | 43.3 ± 0.9 | 36.8 ± 0.8 | 10.7 ± 0.2 | 47.5 ± 0.9 |

spectrometry (HPGe, Prisna). The non-detectable U and Th concentration is a good indication of the purity of the salt because U and Th would stick to clay or other sediment particles. The potassium results of the mixed sample translate to an effective central dose rate of 48.3 ± 1.4 Gy ka$^{-1}$ (mS1 and mS2) driven solely by the decay of $^{40}$K. This is considerable for an environmental dose rate where typical values range from 1 Gy ka$^{-1}$ to 3 Gy ka$^{-1}$ in sediments such as loess or sand or ca. 4 Gy ka$^{-1}$ for playa deposits with intercalated halites [75]. Compared to the mixed, the sylvite samples (sS1 and sS2) exhibited higher potassium concentrations up to ca. 54 %, which resulted in a ca. 20 % higher total dose rate of ca. 58 Gy ka$^{-1}$. In stark contrast, for the blue halite samples (bhS1, bhS1), we measured potassium concentrations of ca. 3.6 ± 0.1 % (bhS2) and 8.4 ± 0.1 % (bhS1). These findings agree with the magnitudes of the specific radioactivity reported by Zelek et al. [19], who measured 13,930 ± 630 Bq kg$^{-1}$ (44.9 ± 2.0 %) for sylvite and 1,582 ± 72 Bq kg$^{-1}$ (5.1 ± 0.2 %) for blue halite from the Kłodawa salt mine.

The central values were calculated per column values. Samples were measured with gamma-ray spectrometry only for comparison.

### 4.6. Attempt to date using the LL method - determining the age

With the $D_e$ values and the dose rate results at hand, we can now attempt to calculate an LL age for our samples in Fig. 7 a) b) using the following equation:

$$A = \frac{D_e}{\dot{D}} = \frac{D_e}{\dot{D}_\alpha + \dot{D}_\beta + \dot{D}_\gamma + \dot{D}_{cosm.}} \tag{19}$$

$A$ is the LL age in ka, $D_e$ is the equivalent dose in Gy, $\dot{D}$ are the dose rate components in Gy ka$^{-1}$ for the different types of irradiations. Given the absence of significant U and Th concentrations, we can set $\dot{D}_\alpha := 0$, and likewise $\dot{D}_{cosm.} := 0$ because of the negligible contribution from cosmic rays in the mine. The remaining dose rate components were corrected for a water content of 1 ± 1 %. We did not consider further dose-rate attenuation factors. The values would result in a LL age for sS2 of 0.018 ± 0.002 ka. For calculating the age of samples bhS1 and bhS2, we will use the $\dot{D}_\gamma$ of the mixture and the $\dot{D}_\beta$ of the blue halite, which gives total dose rates of 19.25 ± 0.03 Gy ka$^{-1}$ (bhS1) and 14.28 ± 0.03 Gy ka$^{-1}$ (bhS2) and ages of 0.034 ± 0.007 ka (bhS1) and 0.061 ± 0.011 ka (bhS2). This leaves us with the LL age of the salts ranging from ca. 18–61 years with millions of years old salt formation. The obtained ages were somewhat consistent for all samples of blue halite and sylvite; however, they were too young concerning the expected formation age (~28 Ma).

## 5. Discussions

The most prominent obstacle while measuring natural LL in minerals seems to be hydration water within the crystal structure, which promotes tunnelling between electrons and recombination centres. This effect prevents the formation of colour centres and can hamper measuring natural LL. The phenomenon can be observed by comparing LL signals from natural minerals in anhydrous and hydrated forms, with a clear advantage in favour of the anhydrous forms (an example for barium chloride can be found in the work of Patil et al. [76]). In our study, we assumed that we were working with anhydrous materials with a residual natural water content of 1–2 %. However, since halite and sylvite are hygroscopic materials, we could not avoid exposing them to short-term contact with ambient air during preparation and just before measuring LL. To assess the significance of the effect of such exposure to moisture further, it would be necessary to conduct comparative studies of natural LL signals measured in situ, which went beyond the scope of this work but can be possible using a portable LL reader (details will be provided in a separate publication).

To measure significant LL, a high concentration of radionuclides in the surrounding environment or within the mineral is generally favourable to generate a sufficiently high annual dose rate. This led us to study the most promising materials – blue halite, proposed by Atari in 1973 [24]. On the other hand, the datable age range of LL is governed by the concentration of *F*-centres, which probably affects them long before they achieve their saturation level. The work of Mador et al. [68] on X-ray irradiated NaCl samples shows that *F*-centres saturate at a concentration of 6 × 10$^{16}$ cm$^{-3}$ to 2 × 10$^{17}$ cm$^{-3}$ under ambient conditions. In the case of salt-dominated evaporites, the saturation of *F*-centre concentration can reach up to 10$^{19}$ cm$^{-3}$ as the structure of such materials is strongly defective (sizeable initial concentration of available vacancies). According to Etzel and Allard [77], the energy required to create one *F*-centre by MeV radiation source in halite is about 85 eV, equivalent to ~ 1.36 × 10$^{-17}$ J. At half the saturation value for the *F*-centres, i.e., about 1 × 10$^{17}$ cm$^{-3}$, thus the total energy that has to be delivered into one cubic centimetre of the sample is ~1.36 J. Assuming that the mass of one cubic centimetre of salt sample is 2.17 × 10$^{-3}$ kg, the total absorbed dose can be calculated as 1.36 J/2.17 × 10$^{-3}$kg ≈ 626.7 Gy. Assuming an average dose rate for sediments of about 3 Gy ka$^{-1}$, the time that will elapse until the assumed level of half the maximum concentration of *F*-centres is reached after around 209 ka. If we assume the level of *F*-centre concentration is about 90 % of the maximum value, then the analogous time will be 376 ka. From these theoretical considerations, the upper age limit for dating by the LL method would be several hundred thousand years for chloride salt

sediments, if the occurrence of aggregated colour centres is avoided. Those numbers still require experimental confirmation. Furthermore, this age value is indeed much lower than that resulting from the saturation values of the LL dose dependence curve for halite. However, this approach seems to carry merit as *F*-centres are involved in the production of the LL signal, and the presence of aggregated centres is undesirable because they essentially lower the determined age without contributing to the LL emission. The practical consequence is that we argue that the concentration of colour centres should be determined for each specific mineral before starting the LL dating procedure. In the future, an attempt should be made to establish a correction factor for the obtained equivalent dose based on the concentration of aggregate colour centres in the tested material. Such a procedure could be carried out based on the age of a given mineral determined by several other methods for comparative purposes; it is currently uncertain whether this approach will be effective, though.

Other critical factors of LL concern the sampling and sample handling procedure, which must ensure protection from light and moisture. In laboratory settings, preparing halite grains for analysis can be challenging due to their solubility and the presence of other saline minerals, which can be reduced by airtight storage and sieving can help to isolate grains from crushed larger crystals. However, access thermal treatments (up to 400 °C) induced significant changes in the LL sensitivity of the studied samples (see Fig. 6), and further refinement of the procedure for resetting the natural LL signal is required in the future. Likewise, the optimal method for zeroing the natural LL signal remains to be determined. Selecting the appropriate solvent and, if necessary, an LL reaction activator allows for the optimal enhancement of the natural LL signal. A measurable LL signal potentially allows for its calibration, which is crucial for determining the equivalent dose and subsequently calculating the age of the given mineral. Hence, optimized experimental conditions are indispensable before proceeding with luminescence measurements, which can be achieved through, e.g., dose recovery tests. With regard to the dose rate, Zhang et al. [2] suggested selecting large crystals to simplify the calculation of internal and external beta radiation contributions, while gamma dose contributions can be assessed through on-site gamma-ray spectrometry. The latter was not carried out in our work but will be considered in future studies.

## 6. Conclusions

In this work, we demonstrated the existence of a natural LL signal in blue halite and an ultraweak natural LL in sylvite. We measured the signal using a photon-counting head on three different measurement systems and an EM-CCD camera setup to record LL emissions during dissolution. To that end, we proposed a preparation method for water-soluble minerals that minimizes the loss of the LL signal from the moment of sampling to the moment of reading the LL signal. The conditions for conducting the LL measurement were optimized to obtain the best signal-to-noise ratio and to achieve the best reproducibility with an LL activator concentration of $5{\cdot}10^{-4}$ mol·dm$^{-3}$ for copper chloride. Regarding the effect of crystal grain size, oxygen content in the solvent and the photobleaching effect on the LL signal in blue halite samples, we found that (1) grinding of the material caused a higher natural LL efficiency than in the unfragmented sample; (2) the oxygen contained in the solvent, do not have a quantitative effect on natural LL; (3) similarly, short daylight exposures of the sample do not cause a measured LL reduction. With these results, we attempted to determine the age of formation using LL, but the obtained results turned out to be significantly underestimating the geological formation of the salt deposit. Using UV–VIS spectrophotometry, we observed numerous absorption bands characteristic of blue halite discoloured by radiation. The significant contribution of absorption bands other than the *F*-band, i.e., aggregate bands, in this material indicates a long time of exposure to ionizing radiation, and the presence of these colour bands may explain the underestimation of the obtained LL ages. This is because the hydrated electrons from the *F*-centre participate in the LL emission, while those from other centres make a marginal contribution, if any. We, therefore, conclude that any electron centre other than the *F*-centre is undesirable for LL age determination because the presence of aggregate centres likely leads to underestimated age results.

Although we could not produce a geological age of the presumed last crystallization of the Morsleben salt using LL, our work provides insight that will allow us and others to continue analogous LL studies to obtain more realistic results. In conclusion, our recommendations for future dating and dosimetry studies are summarized as follows:

- **Material type.** Preferred is the presence of *F*-centres only, avoiding aggregated colour centres. *V*-centres were not tested; however, hole-type centres play an essential role in the LL emission only for water as a solvent. By applying reaction activators (e.g., copper ions), the role of *V*-centres can be omitted, as LL is mainly produced by hydrated electrons with copper ions. Among the evaporites, anhydrous forms of potassium-bearing minerals such as aphthitalite (glaserite), hanksite, langbeinite, nitre (saltpetre), and rinneite (for review see: [78]) seem to be preferable for LL dating.
- **Optimization of the** sampling **method and sample preparation method**. Sampling in dark; preparation with red light; LL measurement as soon as possible from the moment of sample collection; protection of samples against moisture; drying the material for the shortest possible time at the lowest possible temperature (in our case, it did not exceed 50 °C, drying time maximum of 24 h); minimal crushing of the material to avoid generating additional surface vacancies; if the solvent is pure water. When using a reaction activator, crushing the material does not seem to interfere with the natural LL signal.
- **Optimization of the** measurement **of the natural LL signal**. Ensure the appropriate sensitivity of the LL measuring device (detector: photon counting head or sufficiently sensitive CCD camera setup). Selection of the optimal reaction activator (type and concentration, here $5{\cdot}10^{-4}$ mol·dm$^{-3}$) to enhance naturally weak LL signal. Establish the same measurement conditions (sample mass, temperature, solvent volume, dissolution rate) to maintain reproducibility.
- **Determination of equivalent dose and dose rate**. In situ dose rate measurements are preferred to provide reliable dose rate readings in case of deposition matrix heterogeneities. Correction of the dose dependence due to fading and loss of LL information due to aggregated colour centres seems sensible. We recommend performing UV–VIS spectroscopy and/or micro-Ramman tests before conducting LL experiments to verify the population of colour centres in the tested natural minerals. Thus, the optimal sample type, i.e., dominant by *F*-centre, should be selected for dating using the LL.

In summary, our work may have potential implications in geochronology, as alkali halides are found as sedimentary deposits from all geological epochs formed through the evaporation of isolated bodies of seawater or saline lakes. This process follows the deposition of carbonates and gypsum anhydrites and precedes the formation of soluble sulphates and K and Mg chlorides [78]. Although blue halite is not commonly found among salt deposits, chloride minerals seem promising in their luminescent properties due to easy colouration upon ionizing radiation. They could serve as a starting point for systematic evaporite research using the LL method in the geochronological context. This approach may facilitate the exploration of archives and subsurface processes, where only the last hydration event is interesting. This, in turn, offers essential data for understanding paleoclimate and paleoenvironmental changes.

## CRediT authorship contribution statement

**Magdalena Biernacka:** Writing – review & editing, Writing – original draft, Visualization, Validation, Resources, Project administration,

Methodology, Investigation, Funding acquisition, Formal analysis, Data curation, Conceptualization. **Renata Majgier:** Visualization, Validation, Investigation, Formal analysis, Writing – review & editing, Writing – original draft. **Krzysztof Staninski:** Writing – review & editing, Writing – original draft, Visualization, Validation, Methodology, Investigation, Formal analysis. **Małgorzata Kaczmarek:** Validation, Investigation, Formal analysis, Writing – review & editing. **Sylwia Zelek-Pogudz:** Visualization, Investigation, Formal analysis. **Michał Sądel:** Writing – original draft, Visualization, Investigation, Formal analysis, Writing – review & editing. **Katarzyna M. Szufa:** Investigation, Formal analysis, Writing – review & editing. **Hartmut Blanke:** Resources. **Sebastian Kreutzer:** Writing – review & editing, Writing – original draft, Validation, Supervision, Project administration, Methodology, Funding acquisition, Formal analysis, Conceptualization.

## Funding

The research was financed by project 101107989 - Lyoluminescence - HORIZON-MSCA-2022-PF-01. SK was supported through the DFG Heisenberg programme (#505822867). The work done at the IFJ PAN was supported by the National Science Centre, Poland (grant No 2021/43/D/ST5/03042).

## Declaration of competing interest

The authors declare no known competing financial interests, personal relationships, or any other associations, including patents pending, that could have appeared to influence the work reported in this paper.

## Acknowledgements

We thank Annette Kadereit and Paul Dickehut for supporting the sample collection in the salt mine in Morsleben, Jutta Asmuth and Laura Wamsler for performing measurements using the μDose system in Heidelberg, and Clemens Theiler and Jannik Meyer for assisting with the LL experiments. Norbert Mercier measured two salt samples using the gamma-ray spectrometer at Archéosciences Bordeaux (France). We also thank Aleksandra Teresa Wesełucha-Birczyńska for supporting the UV–VIS measurements at Jagiellonian University (Poland).

## Appendix A. Supplementary data

Supplementary data to this article can be found online at https://doi.org/10.1016/j.jlumin.2025.121088.

## Data availability

All data was made open access on Zenodo and is digitally identified by DOI https://doi.org/10.5281/zenodo.14071253.

## References

[1] R.M. Bailey, G. Adamiec, E.J. Rhodes, OSL properties of NaCl relative to dating and dosimetry, Radiat. Meas. 32 (2000) 717–723, https://doi.org/10.1016/S1350-4487(00)00087-1.
[2] J.F. Zhang, C. Yan, L.P. Zhou, Feasibility of optical dating using halite, J. Lumin. 114 (2005) 234–240, https://doi.org/10.1016/j.jlumin.2005.01.009.
[3] D.J. Huntley, D.I. Godfrey-Smith, M.L.W. Thewalt, Optical dating of sediments, Nature 313 (1985) 105–107, https://doi.org/10.1038/313105a0.
[4] R.K. Gartia, Paleothermometry of NaCl as evidenced from thermoluminescence data, Nucl. Instrum. Methods Phys. Res. Sect. B Beam Interact. Mater. Atoms 267 (2009) 2903–2907, https://doi.org/10.1016/j.nimb.2009.06.106.
[5] L. Waldner, Optically Stimulated Luminescence Dosimetry with NaCl Pellets. Dosimetry for Prospective Applications, Lund University, Faculty of Medicine, 2021. Doctoral Thesis (compilation), [Department of Translational Medicine].
[6] K. Ahmad, M.B. Kakakhel, S. Hayat, M. Wazir-ud-Din, M.M. Mahmood, S. Ur-Rehman, M.T. Siddique, M. Munir, S.M. Mirza, Dosimetric properties of thermoluminescent NaCl pellets from Khewra salt mines, Pakistan, Luminescence 37 (2022) 1701–1709, https://doi.org/10.1002/bio.4345.
[7] H. Alghamdi, D. Sanderson, L. Carmichael, A. Cresswell, L. Martin, The use of portable OSL and IRSL measurements of NaCl in low dose assessments following a radiological or nuclear emergency, Front. Public Health 10 (2022) 969829, https://doi.org/10.3389/fpubh.2022.969829.
[8] H.M.S. Alghamdi, D.C.W. Sanderson, A.J. Cresswell, S. Fitzgerald, Radiological or nuclear emergency OSL dosimetry using commonplace salt, Radiat. Meas. 174 (2024) 107141, https://doi.org/10.1016/j.radmeas.2024.107141.
[9] C.P. Fernandes, R.R. Rocca, The effects of heat treatment on the OSL signal in sodium chloride crystals, Radiat. Phys. Chem. 214 (2024) 111251, https://doi.org/10.1016/j.radphyschem.2023.111251.
[10] N.A. Atari, K.V. Ettinger, Lyoluminescent tissue equivalent radiation dosimeter, Nature 247 (1974) 193–194, https://doi.org/10.1038/247193a0.
[11] E. Galand, C. Pagnoulle, J. Niézette, J. Vanderschueren, J. Garsou, Lyoluminescence of inorganic salts, J. Lumin. 75 (1997) 27–33, https://doi.org/10.1016/S0022-2313(97)00100-2.
[12] P.M. Bhujbal, S.J. Dhoble, Lyoluminescence properties of γ-irradiated and $Dy^{3+}$ activated $(K_{0.5}Na_{0.5})Cl$ phosphors for accidental radiation dosimetry, J. Lumin. 136 (2013) 90–94, https://doi.org/10.1016/j.jlumin.2012.10.033.
[13] P.M. Bhujbal, S.J. Dhoble, Lyoluminescence, thermoluminescence and mechanoluminescence studies in γ-ray irradiated $Dy^{3+}$ activated potassium chloride phosphor for accidental radiation dosimetry, Luminescence 27 (2012) 357–361, https://doi.org/10.1002/bio.1358.
[14] P. Sonnenfeld, The color of rock salt – a review, Sediment. Geol. 94 (1995) 267–276, https://doi.org/10.1016/0037-0738(94)00093-A.
[15] G. Calas, L. Galoisy, A. Geisler, Sodium nanoparticles in alkali halide minerals: why is villiaumite red and halite blue? Am. Mineral. 106 (2021) 838–842, https://doi.org/10.2138/am-2021-7917.
[16] C.L.H. Howard, P.F. Kerr, Blue halite, Science 132 (1960) 1886–1887, https://doi.org/10.1126/science.132.3443.1886.
[17] A. Wesełucha-Birczyńska, T. Toboła, L. Natkaniec-Nowak, Raman microscopy of inclusions in blue halites, Vib. Spectrosc. 48 (2008) 302–307, https://doi.org/10.1016/j.vibspec.2008.05.005.
[18] A. Wesełucha-Birczyńska, S. Zelek, K. Stadnicka, Blue halite colour centre aggregates studied by micro-Raman spectroscopy and X-ray diffraction, Vib. Spectrosc. 60 (2012) 124–128, https://doi.org/10.1016/j.vibspec.2011.11.001.
[19] S.M. Zelek, K.M. Stadnicka, T. Toboła, L. Natkaniec-Nowak, Lattice deformation of blue halite from Zechstein evaporite basin: Kłodawa Salt Mine, Central Poland, Min. Pet. 108 (2014) 619–631, https://doi.org/10.1007/s00710-014-0323-9.
[20] S.M. Zelek, A. Wesełucha-Birczyńska, J. Szklarzewicz, K.M. Stadnicka, Spectroscopic properties of halite from Kłodawa salt mine, central Poland, Min. Pet. 109 (2015) 45–51, https://doi.org/10.1007/s00710-014-0348-0.
[21] K. Chruszcz-Lipska, S. Zelek-Pogudz, U. Solecka, M.L. Solecki, E. Szostak, K. K. Zborowski, M. Zając, Use of the far infrared spectroscopy for NaCl and KCl minerals characterization—a case study of halides from Kłodawa in Poland, Minerals 12 (2022) 1561, https://doi.org/10.3390/min12121561.
[22] T. Arun, S.S. Ram, B. Karthikeyan, P. Ranjith, D.K. Ray, B. Rout, J.B.M. Krishna, P. Sengupta, V.S. Parlapalli, Ion beam radiation effects on natural halite crystals, Nucl. Instrum. Methods Phys. Res. Sect. B Beam Interact. Mater. Atoms 409 (2017) 216–220, https://doi.org/10.1016/j.nimb.2017.03.062.
[23] P. Mahadik, N. Pathak, P. Sengupta, Spectroscopic studies on blue halite, J. Lumin. 194 (2018) 327–333, https://doi.org/10.1016/j.jlumin.2017.10.013.
[24] N.A. Atari, K.V. Ettinger, J.H. Fremlin, Lyoluminescence as a possible basis of radiation dosimetry, Radiat. Eff. 17 (1973) 45–48, https://doi.org/10.1080/00337577308232596.
[25] H.Y. Göksu, D.F. Regulla, A. Vogenauer, Reconstruction of gamma dose distribution in salt at radioactive waste disposal site by the water insoluble fraction, Radiat. Protect. Dosim. 47 (1993) 331–333, https://doi.org/10.1093/rpd/47.1-4.331.
[26] J. Seinen, J.C. Groote, J.R.W. Weerkamp, H.W. Den Hartog, Radiation damage in NaCl. II. The early stage of *F* -center aggregation, Phys. Rev. B 50 (1994) 9787–9792, https://doi.org/10.1103/PhysRevB.50.9787.
[27] W.J. Soppe, H. Donker, A. García Celma, J. Prij, Radiation-induced stored energy in rock salt, J. Nucl. Mater. 217 (1994) 1–31, https://doi.org/10.1016/0022-3115(94)90301-8.
[28] N.A. Atari, Lyoluminescence mechanism of gamma and additively coloured alkali halides in pure water, J. Lumin. 21 (1980) 305–316, https://doi.org/10.1016/0022-2313(80)90009-5.
[29] N.A. Atari, Lyoluminescence mechanism of additively and gamma coloured alkali halides in fluorescent and chemiluminescent solutions, J. Lumin. 21 (1980) 387–396, https://doi.org/10.1016/0022-2313(80)90030-7.
[30] H.J. Arnikar, P.S. Damle, B.D. Chaure, B.S. Madhav Rao, Aquoluminescence from gamma-irradiated alkali halides, Nature 228 (1970) 357–358, https://doi.org/10.1038/228357a0.
[31] H.J. Arnikar, P.S. Damle, B.D. Chaure, Aquoluminescence from γ-irradiated alkali halides. II. Spectral analysis and effect of *p* H of the medium, J. Chem. Phys. 55 (1971) 3668–3671, https://doi.org/10.1063/1.1676647.
[32] K.V. Ettinger, K.J. Puite, Lyoluminescence dosimetry part I. Principles, Int. J. Appl. Radiat. Isot. 33 (1982) 1115–1138, https://doi.org/10.1016/0020-708x(82)90239-3.
[33] C.D. Kalkar, Lyoluminescence from gamma-irradiated NaCl, Int. J. Radiat. Appl. Instrument. Part C. Radiat. Phys. Chem. 34 (1989) 729–738, https://doi.org/10.1016/1359-0197(89)90275-0.
[34] V.R. Raikwar, in: S.K. Omanwar, R.P. Sonekar, N.S. Bajaj (Eds.), Borate Phosphor Mechanoluminescence and Lyoluminescence Phosphors, first ed., CRC Press, Boca Raton, 2022, pp. 243–276, https://doi.org/10.1201/9781003207757.

[35] C.D. Kalkar, R. Ramani, Enhanced aqualuminescence from -irradiated NaCl in the presence of activators: $Cu^{2+}$ and $Co^{2+}$ Ions, Radiochem. Radioanal. Lett. 47 (1981) 203–210.

[36] H.J. Arnikar, L.B. Bapat, T.P.S. Pathak, Effect of F → M phototransformation on aquoluminescence from γ-irradiated sodium chloride, J. Chem. Soc. Faraday. Trans. 1 (75) (1979) 844, https://doi.org/10.1039/f19797500844.

[37] B.P. Chandra, R.K. Tiwari, R. Mor, D.P. Bisen, Theoretical approach to the lyoluminescence of alkali halides, J. Lumin. 75 (1997) 127–133, https://doi.org/10.1016/S0022-2313(97)00108-7.

[38] S.J. Dhoble, P.M. Bhujbal, N.S. Dhoble, S.V. Moharil, Lyoluminescence, thermoluminescence and photodecomposition in microcrystalline powder of KCl, KBr, KI and KI:KNO3 crystals, Nucl. Instrum. Methods Phys. Res. Sect. B Beam Interact. Mater. Atoms 192 (2002) 280–290, https://doi.org/10.1016/S0168-583X(02)00477-9.

[39] P. Banerji, H.K. Kundu, D. Banerjee, R. Bhattacharya, The decays of lyoluminescent alkali halides, J. Lumin. 62 (1994) 109–113, https://doi.org/10.1016/0022-2313(94)90337-9.

[40] V. Nayar, P.S. Chowdhary, P.M. Bhujbal, S.J. Dhoble, Studies on the mass and temperature dependence of lyoluminescence intensity of microcrystalline powder of KCl, Luminescence 26 (2011) 324–330, https://doi.org/10.1002/bio.1232.

[41] Y. Zhang, M. Krause, M. Mutti, The Formation and structure evolution of Zechstein (Upper Permian) salt in Northeast German Basin: a review, Open J. Geol. 3 (2013) 411–426, https://doi.org/10.4236/ojg.2013.38047.

[42] F. Neubauer, A. Schorn, C. Leitner, J. Genser, Dating of polyhalite and langbeinite: preliminary results from German Zechstein, in: EGU2013-8385-1, 2013.

[43] H.J. Arnikar, C.D. Kalkar, Spectrum of aquoluminescence from γ-irradiated sodium chloride in the presence of activators: fluorescein and eosin, J. Lumin. 15 (1977) 227–230, https://doi.org/10.1016/0022-2313(77)90021-7.

[44] K. Staninski, M. Kaczmarek, Afterglow luminescence phenomena in the porous anodic alumina, Opt. Mater. 121 (2021) 111615, https://doi.org/10.1016/j.optmat.2021.111615.

[45] K. Staninski, M. Kaczmarek, The effect of the degree of hydration of aluminium oxide thin films on the afterglow luminescence phenomena, Thin Solid Films 802 (2024) 140451, https://doi.org/10.1016/j.tsf.2024.140451.

[46] J. Lee, H.H. Seliger, Quantum yields of the luminol chemiluminescence reaction in aqueous and aprotic solvents, Photochem. Photobiol. 15 (1972) 227–237, https://doi.org/10.1111/j.1751-1097.1972.tb06241.x.

[47] M. Sądel, J. Gajewski, U. Sowa, J. Swakoń, T. Kajdrowicz, P. Bilski, M. Kłosowski, A. Pędracka, T. Horwacik, 3D dosimetry based on LiMgPO4 OSL silicone foils: facilitating the verification of eye-ball cancer proton radiotherapy, Sensors 21 (2021) 6015, https://doi.org/10.3390/s21186015.

[48] J. Schindelin, I. Arganda-Carreras, E. Frise, V. Kaynig, M. Longair, T. Pietzsch, S. Preibisch, C. Rueden, S. Saalfeld, B. Schmid, J.-Y. Tinevez, D.J. White, V. Hartenstein, K. Eliceiri, P. Tomancak, A. Cardona, Fiji: an open-source platform for biological-image analysis, Nat. Methods 9 (2012) 676–682, https://doi.org/10.1038/nmeth.2019.

[49] T. Kolb, K. Tudyka, A. Kadereit, J. Lomax, G. Poręba, A. Zander, L. Zipf, M. Fuchs, The $\mu$Dose system: determination of environmental dose rates by combined alpha and beta counting – performance tests and practical experiences, Geochronology 4 (2022) 1–31, https://doi.org/10.5194/gchron-4-1-2022.

[50] K. Tudyka, S. Miłosz, G. Adamiec, A. Bluszcz, G. Poręba, Ł. Paszkowski, A. Kolarczyk, µDose: a compact system for environmental radioactivity and dose rate measurement, Radiat. Meas. 118 (2018) 8–13, https://doi.org/10.1016/j.radmeas.2018.07.016.

[51] K. Tudyka, K. Kłosok, M. Gosek, A. Kolarczyk, S. Miłosz, A. Szymak, A. Pilśniak, P. Moska, G. Poręba, µDOSE+: environmental radioactivity and dose rate measurement system with active shielding boosted by machine learning, Measurement 234 (2024) 114854, https://doi.org/10.1016/j.measurement.2024.114854.

[52] K. Tudyka, M. Koruszowic, R. Osadnik, G. Adamiec, P. Moska, A. Szymak, A. Bluszcz, J. Zhang, T. Kolb, G. Poręba, µRate: an online dose rate calculator for trapped charge dating, Archaeometry (2022), https://doi.org/10.1111/arcm.12828 arcm.12828.

[53] S. Miłosz, K. Tudyka, A. Walencik-Łata, S. Barwinek, A. Bluszcz, G. Adamiec, Pulse height, pulse shape, and time interval analyzer for delayed $\alpha/\beta$ coincidence counting, IEEE Trans. Nucl. Sci. 64 (2017) 2536–2542, https://doi.org/10.1109/TNS.2017.2731852.

[54] A.J. Cresswell, J. Carter, D.C.W. Sanderson, Dose rate conversion parameters: assessment of nuclear data, Radiat. Meas. 120 (2018) 195–201, https://doi.org/10.1016/j.radmeas.2018.02.007.

[55] P. Guibert, M. Schvoerer, TL dating: low background gamma spectrometry as a tool for the determination of the annual dose, International Journal of Radiation Applications and Instrumentation. Part D, Nucl. Tracks Radiat. Meas. 18 (1991) 231–238, https://doi.org/10.1016/1359-0189(91)90117-Z.

[56] F. Seitz, Color centers in alkali halide crystals, Rev. Mod. Phys. 18 (1946) 384–408, https://doi.org/10.1103/RevModPhys.18.384.

[57] J.H. Schulman, W.D. Compton, Color Centers in Solids, Macmillan, 1962. https://books.google.de/books?id=MjlRAAAAMAAJ.

[58] H.F. Ivey, Spectral location of the absorption due to color centers in alkali halide crystals, Phys. Rev. 72 (1947) 341–343, https://doi.org/10.1103/PhysRev.72.341.

[59] A. Smakula, Über Erregung und Entfärbung lichtelektrisch leitender Alkalihalogenide, Z. Phys. 59 (1930) 603–614, https://doi.org/10.1007/BF01344801.

[60] R. Ramani, Effect of inorganic metal ion impurities on lyoluminescence, Radiat. Eff. 86 (1984) 47–56, https://doi.org/10.1080/01422448408205213.

[61] L.E.G. Eriksson, I. Lundqvist, A. Sonesson, A. Block-Bolten, J.M. Toguri, H. Flood, Quenching effect of oxygen on the light emission produced by dissolution of irradiated sodium chloride in water, Acta Chem. Scand. 16 (1962) 2113–2116, https://doi.org/10.3891/acta.chem.scand.16-2113.

[62] K. Copty-Wergles, R. Nowotny, P. Hille, Triboluminescence of sodium chloride, Radiat. Protect. Dosim. 33 (1990) 339–342, https://doi.org/10.1093/oxfordjournals.rpd.a080825.

[63] B. Lelievre, J.-P. Adloff, Étude de la luminescence accompagnant la dissolution du chlorure de sodium irradié par le rayonnement γ du cobalt 60, J. Phys. France 25 (1964) 789–796, https://doi.org/10.1051/jphys:01964002508-9078900.

[64] R. Nayar, V. Nayar, S.J. Dhoble, Lyoluminescence: recent developments and dosimetric applications, in: Radiation Dosimetry Phosphors, Elsevier, 2022, pp. 455–485, https://doi.org/10.1016/B978-0-323-85471-9.00001-4.

[65] H.J. Arnikar, P.S. Damle, B.D. Chaure, 'Aquoluminescence' from γ-irradiated crystals: effect of isothermal annealing, J. Phys. Appl. Phys. 5 (1972) 1123–1126, https://doi.org/10.1088/0022-3727/5/6/414.

[66] R. Casler, P. Pringsheim, P. Yuster, Stability of color centers in alkali halides, J. Chem. Phys. 18 (1950) 887–891, https://doi.org/10.1063/1.1747792.

[67] H.J. Arnikar, B.S.M. Rao, M.A. Gijare, S.S. Saradesai, Variation of aquoluminescence during the decay and regeneration of thermoluminescence under F-light, J. Chim. Phys. 72 (1975) 654–658, https://doi.org/10.1051/jcp/1975720654.

[68] I.L. Mador, R.F. Wallis, M.C. Williams, R.C. Herman, Production and bleaching of color centers in X-rayed alkali halide crystals, Phys. Rev. 96 (1954) 617–628, https://doi.org/10.1103/PhysRev.96.617.

[69] R.B. Gordon, A.S. Nowick, Structure sensitivity of the X-ray coloration of NaCl crystals, Phys. Rev. 101 (1956) 977–983, https://doi.org/10.1103/PhysRev.101.977.

[70] A.S. Murray, A.G. Wintle, Luminescence dating of quartz using an improved single-aliquot regenerative-dose protocol, Radiat. Meas. 32 (2000) 57–73, https://doi.org/10.1016/S1350-4487(99)00253-X.

[71] R. Casler, P. Pringsheim, P. Yuster, *V* -centers in alkali halides, J. Chem. Phys. 18 (1950) 1564–1571, https://doi.org/10.1063/1.1747541.

[72] R. Majgier, M. Biernacka, R. Smyka, A. Mandowski, Analysis of OSL decay characteristics for beta-irradiated potassium chloride samples, Radiat. Meas. 106 (2017) 67–72, https://doi.org/10.1016/j.radmeas.2017.05.006.

[73] N.A. Atari, K.V. Ettinger, On the lyoluminescence of irradiated alkali halides, Radiat. Eff. 26 (1975) 39–41, https://doi.org/10.1080/00337577508237417.

[74] R.F. Galbraith, R.G. Roberts, Statistical aspects of equivalent dose and error calculation and display in OSL dating: an overview and some recommendations, Quat. Geochronol. 11 (2012) 1–27, https://doi.org/10.1016/j.quageo.2012.04.020.

[75] W. Han, Z. Ma, Z. Lai, E. Appel, X. Fang, L. Yu, Wind erosion on the north-eastern Tibetan Plateau: constraints from OSL and U-Th dating of playa salt crust in the Qaidam Basin, Earth Surf. Process. Landforms 39 (2014) 779–789, https://doi.org/10.1002/esp.3483.

[76] S.F. Patil, D. Ravishankar, P.J. Bhatia, Chemical effects induced by γ-irradiated barium chloride in aqueous medium, Int. J. Appl. Radiat. Isot. 35 (1984) 1095–1098, https://doi.org/10.1016/0020-708X(84)90140-6.

[77] H.W. Etzel, J.G. Allard, Color center formation in sodium chloride, Phys. Rev. Lett. 2 (1959) 452–454, https://doi.org/10.1103/PhysRevLett.2.452.

[78] J.K. Warren, Evaporite deposits, in: Encyclopedia of Geology, Elsevier, 2021, pp. 945–977, https://doi.org/10.1016/B978-0-08-102908-4.00165-X.